The Journal of Chemical Physics

RESEARCH ARTICLE | APRIL 26 2022

Modeling thermodiffusion in aqueous sodium chloride solutions—Which water model is best?

Alice J. Hutchinson ; Juan F. Torres ; Ben Corry

Check for updates

J. Chem. Phys. 156, 164503 (2022)
https://doi.org/10.1063/5.0088325

View Online
Export Citation

25 March 2024 00:54:31

Boost Your Optics and Photonics Measurements

Zurich Instruments

Find out more

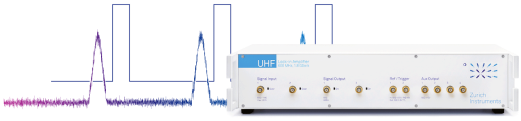

AIP Publishing

The Journal of Chemical Physics ARTICLE scitation.org/journal/jcp

Modeling thermodiffusion in aqueous sodium chloride solutions—Which water model is best?

Cite as: J. Chem. Phys. 156, 164503 (2022); doi: 10.1063/5.0088325
Submitted: 15 February 2022 • Accepted: 7 April 2022 •
Published Online: 26 April 2022

View Online Export Citation CrossMark

Alice J. Hutchinson,[1] Juan F. Torres,[2] and Ben Corry[1,a)]

AFFILIATIONS

[1] Research School of Biology, Australian National University, Canberra, Australia
[2] School of Engineering, Australian National University, Canberra, Australia

[a)] **Author to whom correspondence should be addressed:** ben.corry@anu.edu.au

ABSTRACT

Thermodiffusion is the migration of a species due to a temperature gradient and is the driving phenomenon in many applications ranging from early cancer detection to uranium enrichment. Molecular dynamics (MD) simulations can be a useful tool for exploring the rather complex thermodiffusive behavior of species, such as proteins and ions. However, current MD models of thermodiffusion in aqueous ionic solutions struggle to quantitatively predict the Soret coefficient, which indicates the magnitude and direction of species migration under a temperature gradient. In this work, we aim to improve the accuracy of MD thermodiffusion models by assessing how well different water models can recreate thermodiffusion in a benchmark aqueous NaCl solution. We tested four of the best available rigid non-polarizable water models (TIP3P-FB, TIP4P-FB, OPC3, and OPC) and the commonly used TIP3P and SPC/E water models for their ability to predict the inversion temperature and Soret coefficient in 0.5, 2, and 4M aqueous NaCl solutions. Each water model predicted a noticeably different ion distribution yielding different inversion temperatures and magnitudes of the Soret coefficient. By comparing the modeled Soret coefficients to published experimental values, we determine TIP3P-FB to be the water model that best recreates thermodiffusion in aqueous NaCl solutions. Our findings can aid future works in selecting the most accurate rigid non-polarizable water model, including water and ion parameters for investigating thermodiffusion through MD simulations.

Published under an exclusive license by AIP Publishing. https://doi.org/10.1063/5.0088325

25 March 2024 00:54:31

I. INTRODUCTION

Temperature gradients can induce the movement of a species within a convectionless solution,[1] much like concentration gradients induce Fickian diffusion. This effect, known as thermodiffusion (or thermophoresis or the Soret effect), was first observed over 150 years ago when both Charles Soret and Carl Friedrich Wilhelm Ludwig independently observed that salty solutions in non-isothermal environments built up non-homogeneous ion concentrations.[2] Since then, thermodiffusion has been observed in all kinds of mobile mixtures of gases and liquids, including aqueous electrolytes,[3,4] colloidal suspensions,[5] hydrocarbons,[6] rarefied gases, and plasma.[7,8] Furthermore, thermodiffusion is the driving phenomenon in many applications, including early cancer detection[9] and uranium enrichment.[10] Although the terms thermodiffusion and thermophoresis are sometimes used inconsistently, in general, thermodiffusion is used in reference to the movements of low molecular weight solutes, such as ions in aqueous solutions, and thermophoresis is used in reference to larger macromolecules or colloids.

Despite the rich history of observation, there is no universal explanation as to why thermodiffusion occurs. Consequently, the migration of species is described using a phenomenological model that considers the competition between thermodiffusion due to a temperature gradient and Fickian diffusion that opposes concentration gradients. In a binary mixture, the macroscopic mass diffusion, J, of a thermodiffusive species is described by the addition of these two diffusive currents[1] and described as

$$J = -\rho D \nabla c - \rho c(1-c) D_T \nabla T. \quad (1)$$

Here, ρ is the solution density, D represents the isothermal mass diffusion coefficient that opposes the concentration gradient (i.e. Fickian diffusion), c is the molar fraction (or mass fraction) of the diffusing species, T is the temperature of the solution, and D_T is the thermodiffusion coefficient.

The steady-state separation of species in the mixture occurs when thermodiffusion and Fickian diffusion are balanced, i.e. $J = 0$ in Eq. (1). The Soret coefficient, S_T, describes the magnitude and

Published under an exclusive license by AIP Publishing

thermal preference of the species diffusion and is defined as the ratio of thermodiffusion and Fickian diffusion coefficients, i.e., (assuming that a temperature gradient is only in one dimension)

$$S_T = \left.\frac{D_T}{D}\right|_{J=0} = \frac{-1}{c(1-c)}\left.\frac{dc}{dT}\right|_{J=0}. \quad (2)$$

Typically the Soret coefficient of a solute is positive, meaning thermodiffusion causes the species to diffuse toward the colder region. Interestingly though, thermodiffusion can cause some solutes, including but not limited to ions,[3,11,12] colloids,[13–15] polymers,[13,14,16] charged nanoparticles,[5,14,17] proteins,[14,18,19] DNA,[14,20] and vesicles,[21] to diffuse either toward warmer regions (thermophilic, negative S_T) or colder regions (thermophobic, positive S_T), depending on the local temperature and concentration of the solution. The temperature at which this behavioral change occurs is called the inversion temperature, T_0. This behavior is thought to only occur in solutions with a strong coupling between the migrating particle and the thermal environment.[22] The sign of the Soret coefficient reflects the thermal preference of the diffusive species, as shown in Fig. 1.

Molecular dynamics (MD) simulations have previously been used to reproduce the thermodiffusive behavior of various solutions, including binary solutions of hydrocarbons,[23–26] argon and krypton,[27] water, methanol, ethanol, dimethyl-sulfoxide and acetone,[28,29] aqueous electrolytes,[12,30–32] urea,[33] and DNA fragments.[30] Previously, MD simulations have been shown to predict the correct trend and order of magnitude of the Soret coefficient and inversion of thermal preference for $[Na^+, K^+, Li^+]\,Cl^-$ aqueous solutions.[12,31,32] To improve predictions of thermodiffusion, the accuracy limitations of MD modeling must be considered. MD is based on classical mechanics and, therefore, inherently approximates real-world molecules and their behavior. In an aqueous electrolyte MD simulation, the major approximations lie upon the choice of the ion and water models (force fields), which define the structure and interactions of these molecules. Therefore, ion and water models are key players in the accurate representation of the modeled solution and its thermodiffusive behavior. It has been shown that ion force fields (with the same water model) minimally affect the thermodiffusive behavior of $[NaCl]_{aq}$ and $[KCl]_{aq}$ solutions.[12,31] However, the effect of the water model has not previously been investigated, despite a greater accuracy in predicting thermodiffusion likely to be achieved by selecting the most appropriate water models in the MD simulation.

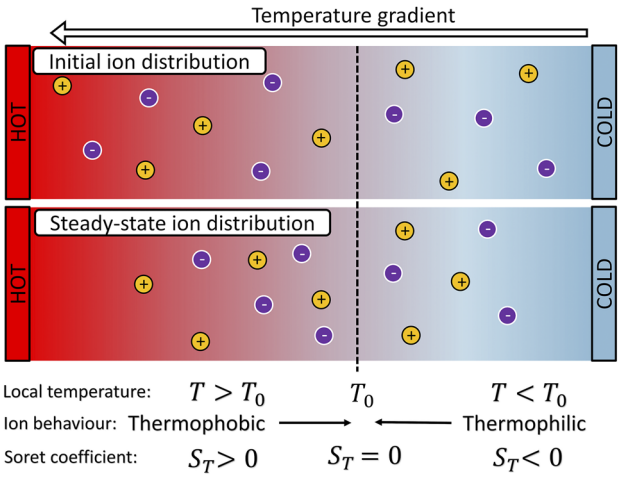

FIG. 1. Depiction of thermophilic and thermophobic behavior of an aqueous NaCl solution under a linear temperature profile that encompasses an inversion temperature. The direction of thermally driven ion diffusion is indicated by the sign of the Soret coefficient, S_T, and depends on whether the local temperature of the solution, T, is greater or less than the inversion temperature, T_0.

Given the importance of the water model in defining the forces leading to thermodiffusion, we sought to test which model is the most appropriate for modeling thermodiffusion of $[NaCl]_{aq}$ solutions. This solution was chosen because its Soret coefficient has been accurately measured,[12] its thermodiffusive behavior is well known,[11] and it is a broadly relevant simple solution for both biological and industrial systems and to other projects in our laboratory. While the exact mechanism of thermodiffusion is not well understood, multiple sources emphasize the importance of hydrogen bond structures, solute–water interactions, and hydration entropy in defining thermodiffusive behavior.[20,32,34] The water model and its associated ion parameters define the molecule structure and the water–water, ion–ion, and water–ion interactions in the solution and are therefore integral to accurately recreating thermodiffusion. Water models come in a range of types with rigid, non-polarizable water models being by far the most commonly used in MD simulations. They are simple, computationally inexpensive, and have previously been used in modeling thermodiffusion.[12,30–32] They represent water molecules as rigid bodies of a given number of points that interact via electrostatic and van der Waals potentials, which are parameterized against reference data, such as experimentally measured properties or higher level calculations.

In this work, the thermodiffusive behavior of three- and four-point models from two of the best performing water model families were tested: TIPnP-FB (which focuses on experimental reference data[35]) and OPCn (which focuses on quantum mechanically calculated reference data[36,37]). We also tested two commonly used models: TIP3P,[38] an old but regularly used water model that is expected to perform more poorly, and SPC/E,[39] the three-point water model commonly used in other MD thermodiffusion works.[12,32] These commonly used models serve as a good comparison point between results from this work and the literature. Specifically, we sought to compare the performance of the chosen water models in reproducing the inversion temperature of 0.5 M $[NaCl]_{aq}$ solutions and the Soret coefficient of 0.5, 2, and 4 M $[NaCl]_{aq}$ solutions, as compared to the experimental values obtained by Römer *et al.*[12]

II. METHODS

A. Model setup

A typical model setup is shown in Fig. 2. The MD model consisted of ~47 000 atoms (15 000 water molecules and <2000 ions), contained in a rectangular prism (volume 50 × 100 × 100 Å) with periodic boundaries. The system size and boundaries were chosen to ensure simulation of bulk solution dynamics with no edge effects while minimizing computational effort. The length of all axes were larger than the Debye shielding length of any modeled

25 March 2024 00:54:31

Published under an exclusive license by AIP Publishing

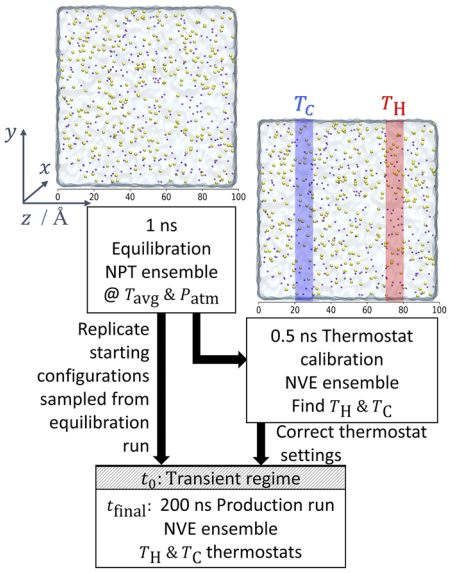

FIG. 2. Simulation strategy for reproducing thermodiffusion in an MD model of aqueous sodium chloride subjected to temperature control with two thermostats. A front-facing visualization of the model is depicted with the volume occupied by water molecules shown graphically in light gray, sodium ions shown in yellow, and chloride ions in purple. Cold (T_C) and hot (T_H) thermostats of width 10 Å (highlighted blue and red regions, respectively) are centered at z = 25 Å and z = 75 Å to achieve a quasi-linear temperature profile across the z axis. The simulation strategy has three main steps: equilibration in a constant number of atoms, pressure, and temperature (NPT) ensemble; thermostat calibration in a constant number of atoms, volume, and energy (NVE) ensemble; and production run also in an NVE ensemble.

ion to avoid charged particles interacting electrostatically with their periodic images.

Water molecules were modeled using the structure and geometry parameters of the six water models sourced from the corresponding literature: TIP3P-FB,[35] TIP4P-FB,[35] OPC3,[37] OPC,[36] SPC/E,[39] and TIP3P.[38] Ion parameters are most accurate when used in conjunction with the water model that they were parameterized with. Therefore, for TIP3P-FB, TIP4P-FB, OPC3, and OPC, the monovalent ion parameters for Na^+ and Cl^- ions were sourced from Ref. 40, having been fit to each water model to recreate the ion hydration free energy. Monovalent ion parameters that match TIP3P were sourced from Ref. 41. Monovalent ion parameters for SPC/E were used identically to those in the MD simulations of Römer *et al.*[12] sourced from the combined works of Dang, Garrett, and Smith.[42–45] Sourced values are listed in Tables S1 and S2.

B. Temperature regulation

Temperature gradients used to measure thermodiffusion in physical experiments are typically on the order of 1 °C cm^{-1}, whereas in MD simulations, they are usually on the order of 1 °C $Å^{-1}$. While non-physical, these large gradients are not thought to impact the thermodiffusive behavior of the system.[12,29,31,32]

To achieve a non-uniform temperature profile within the system, two spatially defined thermostats were applied. The thermostat method was designed by Belkin *et al.*[30] by altering a pre-existing feature of the Nanoscale Molecular Dynamics (NAMD) simulation software. At each simulation time step (every 2 fs), any water molecule to enter a defined thermostat region had a probability of its relative velocity being reassigned via a collision with the temperature

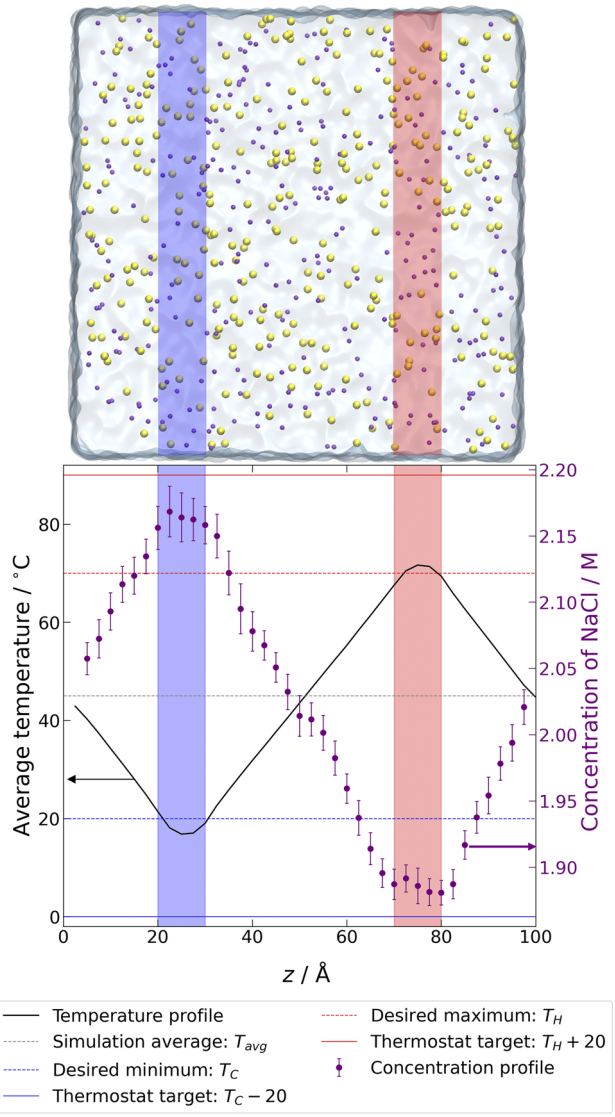

FIG. 3. MD model of a 2.0 M aqueous NaCl solution with a linear temperature profile spanning ~20–70 °C. The ion concentration increased as the temperature decreases, demonstrating thermodiffusion of sodium and chloride ions *in silico*. The model volume (top) is occupied by water molecules (light gray), sodium ions (yellow), and chloride ions (purple). A cold and a hot thermostat of width 10 Å (highlighted blue and red regions, respectively) are centered at z = 25 Å and z = 75 Å. Thermostat target temperatures were set 20 °C more extreme than the desired minimum and maximum temperature. The achieved temperature (black solid line) and concentration profiles (purple markers) in the solution are plotted. The temperature gradient is approximately linear between thermostats and has a gradient of ~1.1 °C $Å^{-1}$. The ion concentration profile is averaged over (t_0 = 5, t_{final} = 200) ns of simulation time, corresponding to the steady-state regime. The error bars represent the standard error in the mean concentration considering temporal fluctuations. The TIP3P-FB water model was used in this simulation.

25 March 2024 00:54:31

Published under an exclusive license by AIP Publishing

bath (that is, a velocity sampled from a Maxwellian distribution for the set temperature) by Lowe–Andersen dynamics with a collision frequency of 50 ps^{-1}. The average temperature across the system was determined directly from the particle velocities and, as seen in Fig. 3 and Fig. S1, is approximately linear in the region between the thermostatted regions. Note that Non-equilibrium MD simulations, such as this one, do not achieve linear temperature gradients.[46] The hot and cold thermostat regions were spaced symmetrically about the midpoint of the z-axis and defined in a volumetric grid with a grid size of 1.0 Å. Two coordinate files were created with all water molecules flagged with an occupancy of 1.0 and a beta value of the thermostat target temperature. Thermostats were only active on the water molecules in the system and, therefore, did not directly alter the velocities of the diffusing ions under investigation.

It was found that the temperature profile achieved within the simulation depended on the width of the thermostats, the thermostat target temperatures, the ion concentration, and the water model being used. As there were both a hot and cold thermostat working simultaneously, the maximum and minimum temperatures of the system were less than the target temperature defined in the thermostats (see Fig. 3). Thermostat target temperatures were calibrated to each specific model setup to achieve consistent temperature profiles across simulations (Fig. S1). The width of the thermostat did not affect the approximate linearity of the steady-state temperature profile (Fig. S2). Therefore, a 10 Å width was used in all simulations as it is larger than the mean free path of the water molecules (~7 Å) but small enough for observing thermodiffusion in the computational domain outside the temperature-controlled region.

C. Simulation time step and non-bonded interactions

All simulations were conducted with NAMD[30,47] and a time step of 2 fs. The short-range nonbonded interactions were calculated every 2 fs, while the full electrostatic field of the system was evaluated every 4 fs, a multiple time step approach supported by NAMD. Van der Waals interactions were truncated smoothly at a distance 12 Å from each atom, with truncation beginning a distance 10 Å from each atom. All pairs of bonded atoms connected by less than two bonds were excluded from non-bonded interactions, as dictated by the force field choice. Therefore, no inter-molecular interactions were modeled within water molecules. Electrostatics under periodic boundary conditions were calculated directly within a distance 12 Å from each atom. Beyond 12 Å, electrostatics were calculated with the particle mesh Ewald scheme using all default settings and a grid size of $\{X = 54, Y = 108, Z = 108\}$ Å.

D. Simulation systems and equilibration

The overall simulation strategy is shown graphically in Fig. 2 and detailed as follows. Initial configurations of the aqueous solutions had molecules placed randomly in the simulation system and were energetically minimized for 100 steps using a conjugate gradient and line search algorithm. To allow these molecules to adopt a more natural organization, an equilibration simulation was run at constant temperature, T_{avg}, and pressure of 1.013 25 bar. An equilibration simulation length of 1 ns was found to be sufficient for the volume of the system to reach a steady equilibrium value. The temperature was maintained using Langevin dynamics with a damping coefficient of 1 ps^{-1}. Langevin dynamics introduced additional damping and random forces to the atoms of the system to maintain a velocity distribution centered around T_{avg}. The pressure was maintained using Nosé–Hoover Langevin piston control. The Langevin piston was employed with a period of 100 fs and a decay of 50 fs.

The last frame from the equilibration simulation was used as the first frame in a set of thermostat calibration simulations. The thermostat calibration simulations were run in a constant volume environment for 0.5 ns, long enough to reliably quantify the gradient of the time-averaged temperature profile. The thermostats were set to target temperatures that center around the simulation average temperature T_{avg}. The resulting temperature profile through the system was calculated from the atom positions and velocities at each frame, as described in Sec. II E (data analysis). The thermostat target temperatures that achieve the desired temperature values and gradient were then used for the production run of the simulation.

Independent replicates of the simulation were created before the data production run. Initial coordinates for each replicate were randomly sampled from the last 0.25 ns of the equilibration simulation. The initial velocities of replicates were randomly assigned to atoms to recreate a temperature distribution centered around T_{avg}. The production run of the simulation lasted 200 ns with constant volume and two thermostats applied. t_0 (ns) corresponds to the time taken for the concentration profile to reach a steady state. Steady state concentration and temperature profiles were analyzed in the simulation time interval of $t \in [t_0, t_{final}]$, as described below.

TABLE I. Thermal conditions and number of replicates for the simulation runs in this study. The simulation time for each run was set to t_{final} = 200 ns.

Average ion concentration [NaCl]/M	Average temperature T_{avg}/°C	Desired temperature range $[T_C, T_H]$/°C	Replicates	Purpose
0.5	10	[−10, 30]	5	T_0
0.5	30	[5, 55]	3	$S_T(T)$
0.5	45	[20, 70]	3	$S_T(T)$
0.5	70	[45, 95]	3	$S_T(T)$
2	45	[20, 70]	3	$S_T(T)$
4	45	[20, 70]	3	$S_T(T)$

25 March 2024 00:54:31

Published under an exclusive license by AIP Publishing

Distinguishing between the time required to reach steady state and the time required to calculate a meaningful average of the ion concentration profile was challenging. Therefore, the time required to reach steady state (t_0) was determined by considering two factors. First, we considered a scaling law approach inspired by Diaz-Marquez and Stirnemann,[29]

$$t_0 \sim \mathcal{O}\left(\frac{L_z^2}{DN}\right), \tag{3}$$

where t_0 is the time taken for N diffusing particles to reach a steady state concentration profile, $\frac{L_z}{2}$ is the length the temperature gradient spans (Å), D is the solute diffusion coefficient (Å^2 ns^{-1}), and N is the number of diffusing solute particles. Second, we considered the independence of the final results on the choice of t_0.

To make a conservative upper bound of t_0 for NaCl concentration profiles, the diffusion coefficient, D, of NaCl was measured in a simulation of $T_{avg} = 10\,^\circ$C and $C = 0.5$ M ($N = 298$ ions). It was found that $500 < D < 1150$ Å^2 ns^{-1}, consistent with experimental results.[11] Using Eq. (3) and $D \sim \mathcal{O}(100$ Å^2 ns$^{-1})$, $L_z = 100$ Å, and $N \geq 298$ ions, the upper bound was found to be $t_0 \leq 0.34$ ns. Accounting for the rough nature of this scaling law, the upper bound was conservatively increased to an estimate of $t_0 = 5$ ns applied to all simulations. The independence of the computed inversion temperature in each simulation to the choice of t_0 is shown in Fig. S3.

A summary of the simulation conditions (average concentration, average temperatures and desired temperature ranges) is shown in Table I. These simulations were constructed for all water models and run with three or five independent replicates of duration $t_{final} = 200$ ns.

E. Data analysis

The production portion of each simulation trajectory was used to calculate the average concentration and temperature profiles over the z-axis of the simulation. To do this, the z-axis was discretized into bins of width $h = 2.5$ Å, and the number of molecules $N_s(z_i, t)$ and their velocities (v_{xj}, v_{yj}, v_{zj}) were recorded in each bin for each timeframe using a Fortran script. The concentration of each species at each time step was calculated from

$$C_s(z_i, t) = \frac{N_s(z_i, t)}{VN_A}, \tag{4}$$

where $s \in \{H_2O, Na^+, Cl^-\}$ is the number of molecules of species s in the subvolume, $V = L_x \times L_y \times h = 2 \times 10^{-24}$ L is the volume of the

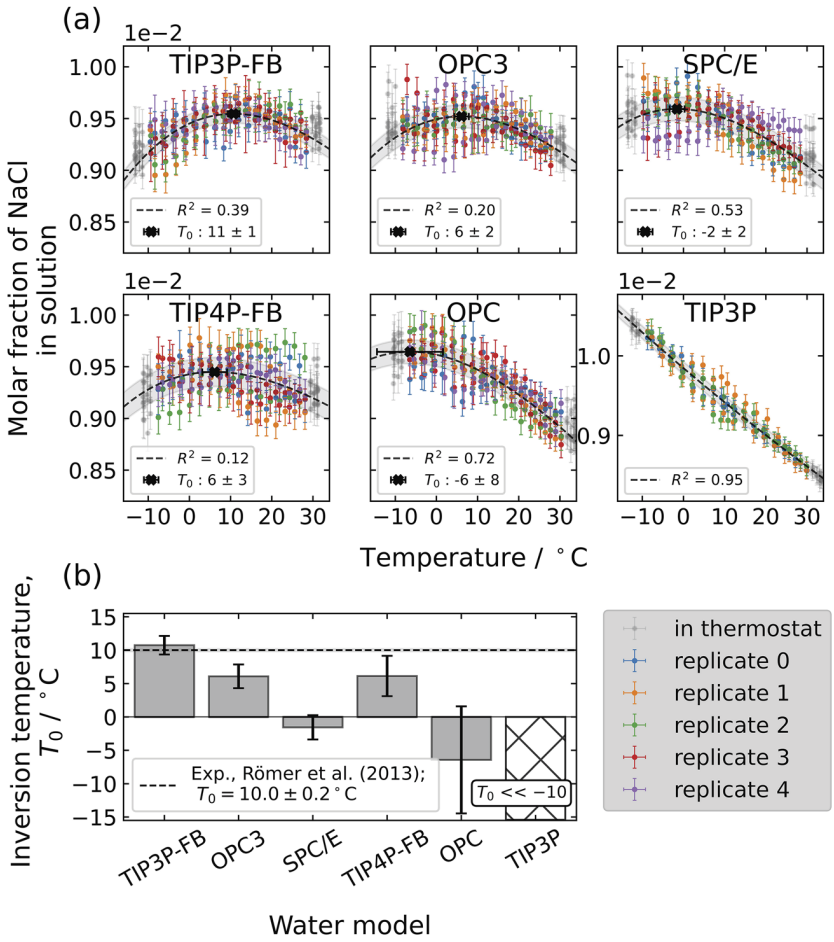

FIG. 4. Inversion temperature of a 0.5 M $[NaCl]_{aq}$ solution predicted by different rigid non-polarizable water models. (a) Molar fraction of NaCl against temperature for five independent replicates of each water model. The molar fraction data between thermostats are fit to the theoretical functional form in Eq. (6) and shown as a dotted gray line. Data points shown as gray dots lie within the thermostatted regions and were excluded from the fitting. A measure of fitting quality or spread in the data is shown by an R^2 value and the mean absolute error (shaded gray area) between the fit and the data points of all replicates. The predicted inversion temperature, T_0, and the error in this fitting parameter are shown as a black bar and reported in the legend to one significant figure. (b) Summary of predicted inversion temperatures and comparison to the experimental value obtained by Römer *et al.*[12] at 0.5 mol kg^{-1} (note that simulation solutions have a comparable but non-identical concentration of 0.5 M = 0.53 mol kg^{-1}). TIP3P notably did not yield an inversion temperature within the tested temperature range.

25 March 2024 00:54:31

Published under an exclusive license by AIP Publishing

subvolume, and $N_A = 6.022\,14 \times 10^{23}$ mol^{-1} is Avogadro's number, and the position of a water molecule was defined by the position of the oxygen atom. The temperature was calculated using Eq. (5) where each ion had three degrees of freedom (Df), each rigid water molecule had six degrees of freedom, and $k = 1.3807 \times 10^{-23}$ JK^{-1} is the Boltzmann constant,

$$T(z_i, t) = \frac{1}{2k} \sum_{j=1}^{N_i} \frac{2m_j(v_{xj}^2 + v_{yj}^2 + v_{zj}^2)}{Df_j}. \tag{5}$$

The steady state behavior of an aqueous electrolyte solution under a temperature gradient was assessed by averaging the concentration and temperature profiles from each trajectory across all frames considered in the steady state. To remove the arbitrary spatial dimension from the analysis, the average concentration $\bar{C}_s(z_i)$ and average temperature $\bar{T}_s(z_i)$ profiles are combined to create an average concentration against the average temperature profile $\bar{C}_s(\bar{T})$. As the Na^+ and Cl^- ions diffuse together at the macro-scale level due to their electrostatic attraction, the combined ion concentration $C_{NaCl}(T)$ is reported in further analyses. The molar fractions of the ions were calculated from the ratio of the ion concentration to the sum of the ion and water concentrations.

There were large fluctuations in the instantaneous values of $C_{NaCl}(z_i, t)$ due to there being a finite number of ions in the simulation with pronounced random motion. To better represent the variation in the concentration profile, the standard deviation and standard error in the mean of the average ion concentration profiles $\bar{C}_{NaCl}(z_i)$ were calculated from a subset of decorrelated frames. The decorrelation analysis was completed using the `timeseries` module of the `pymbar` package.[48,49] All data analysis was completed using Fortran scripts or in Jupyter Notebooks[50] using the packages `pandas`, `numpy`, `math`, `scipy.optimise`, `scipy.stats`, and `pymbar`.

Data points that fall within the thermostatted regions were excluded from the calculation of the inversion temperature and Soret coefficient. The inversion temperature, T_0, was found from the maximum of the NaCl molar fraction concentration profile (see Fig. 4). To obtain a physically meaningful and smooth NaCl concentration profile, the combined molar fraction data were fit to its theoretical functional form,

$$c_{\text{theory}}(T) = c_0 \exp\left[-S_T^\infty \left(T\tau e^{\frac{T_0 - T}{\tau}} + k\right)\right]. \tag{6}$$

The empirical fit was first proposed by Iacopini *et al.*[14] and its use inspired by Di Leece *et al.*[32] It contains four fitting parameters: T_0 is the temperature at which $S_T = 0$, S_T^∞ is the Soret coefficient at the limit of $T \to \infty$, τ is a measure of the rate at which S_T varies with T, and k is a non-physical fitting parameter. An estimate of the inversion temperature and its associated uncertainty were obtained explicitly from the fitting parameter T_0 in the theoretical functional form. Equation (6) was fit to the molar fraction data using the python package `scipy.optimise` and the function `curve_fit` using a least squares fitting method with parameter boundary conditions (see Table S3).

The predicted Soret coefficient vs temperature was determined by first obtaining estimates of the parameters S_T^∞, T_0, and τ as above for each simulation replicate and then used in the corresponding functional form

$$S_T(T) = S_T^\infty \left(1 - e^{\frac{T_0 - T}{\tau}}\right). \tag{7}$$

The final estimate of the Soret coefficient over temperature was reported as an average and standard deviation of the Soret coefficients measured from three simulation replicates.

III. RESULTS

A. Thermodiffusive behavior

An example of the average steady-state temperature and ion concentration profiles from a simulations run is shown in Fig. 3. The concentration of ions increases as the temperature decreases, showing the ions exhibiting realistic thermophobic behavior in this region above the expected inversion temperature. The temperature within the simulation reached a steady approximately linear profile between the hot and cold thermostats within 0.5 ns of simulation time, converging much faster than the concentration profiles (see Fig. S4). This is consistent with the diffusion of heat being more rapid than the diffusion of mass. No explicit energy conservation algorithm was employed. The instantaneous total energy and temperature of the system fluctuated over the simulation time frame, but there was no overall change to the average total energy and temperature of the system. We, therefore, report reasonable energy conservation achieved by the Lowe–Andersen thermostats and no thermal slip, indicating that energy injection in the hot thermostat was compensated by energy withdrawal in the cold thermostat. Importantly, mass diffusion in the simulation was observed as a result of the imposed temperature gradient, demonstrating thermodiffusion. The convergence of the ion concentration profile was more challenging to characterize than for the temperature profile (Fig. S5). This was due to the large uncertainty associated with the small number of ions in the simulation, resulting in large fluctuations in the instantaneous local concentration. As noted in Sec. II, this meant that replicate simulations of relatively long duration were required to generate reliable averages, as well as an approach to determine the time required to reach steady state and to remove correlated data in the uncertainty calculations.

B. Inversion temperature

The inversion temperature is a key trait of thermodiffusion in aqueous electrolytes. Therefore, it is a good benchmark for assessing the accuracy of the chosen water models. For a 0.5 mol kg^{-1} $[NaCl]_{aq}$ solution, the inversion temperature was experimentally reported as 10 °C by Römer *et al.*[12] To determine how well each water model can predict this inversion behavior, simulations of 0.5 M $[NaCl]_{aq}$ (0.53 mol kg^{-1}) were set with an average temperature of $T_{avg} = 10$ °C and a temperature gradient of ~1.1 °C Å^{-1}, spanning the temperature range $-10\,°C < T < 30\,°C$. These simulation conditions were set for all water models, with five models (TIP3P-FB, TIP4P-FB, OPC3, OPC, and SPC/E) run with five independent replicates of duration $t_{final} = 200$ ns. As TIP3P replicates showed significantly less variation in the ion concentration profiles within and between replicates, only

25 March 2024 00:54:31

Published under an exclusive license by AIP Publishing

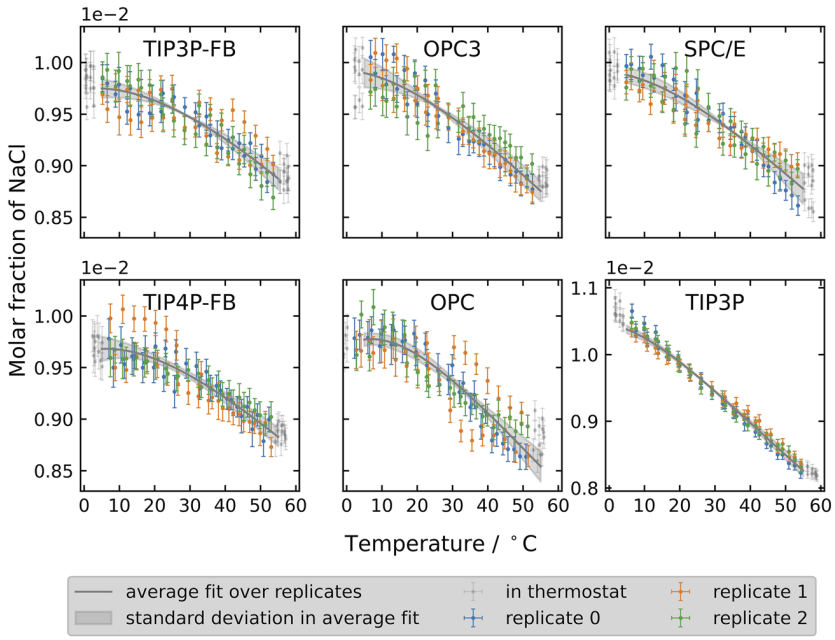

FIG. 5. Molar fraction profile of 0.5 M [NaCl] solution simulated across a temperature range of [5, 55] °C for each water model. Data from independent replicates of simulations are shown with blue, orange, and green dots with an average and standard error in the mean. Data points shown as gray dots lie within the thermostatted regions and were excluded from the fitting. The gray dotted line shows the average fit of Eq. (6) to the data. The standard deviation in the average fit is shown shaded in gray.

three replicates of TIP3P were run for a duration of t_{final} = 120 ns (to conserve computational resources) with no adverse effect on the certainty of the result.

As shown in shown in Fig. 4(a), all water models, except TIP3P, predicted a molar fraction profile with distinct curvature and evidence of a maximum in the temperature range $T \in [-10, 30]$ °C. The occurrence of a maximum in the molar fraction profile demonstrates that these water models can predict the inversion behavior in the NaCl solution. The molar fraction profile of TIP3P was linear in temperature, and hence, TIP3P did not yield an inversion temperature within the tested range.

The molar fraction profiles of TIP4P-FB showed the most variation among replicates of the water models presented in Fig. 4(a). This presents a broader range for isolating a maximum in the curve

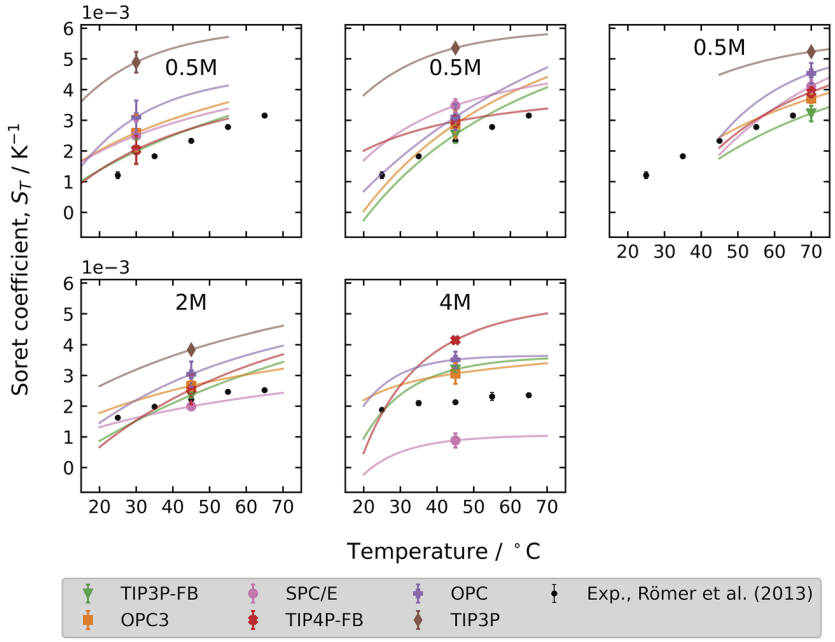

FIG. 6. Soret coefficient as a function of temperature for each water model in simulations of 0.5 M (0.53 mol kg^{-1}) (three temperature ranges), 2 M (2.24 mol kg^{-1}), and 4 M (4.88 mol kg^{-1}) NaCl. The black dots in each plot show the experimentally measured value of the Soret coefficient from Ref. 12 at corresponding comparable solution concentrations of 0.5, 2, and 4 mol kg^{-1}. Soret coefficients (average over three replicates ±standard deviation) from each water model are shown as an emphasized data point at the simulation average temperature, and the shape of the $S_T(T)$ curve is plotted by a solid line.

25 March 2024 00:54:31

Published under an exclusive license by AIP Publishing

and larger uncertainty in the fit between the data and Eq. (6). Equation (6), derived from the well-used empirical fit of the Soret coefficient against temperature,[14] fits the data of the other water models reasonably well and fits the data of TIP4P-FB at other average temperatures and concentrations (see Fig. 5 and Figs. S7–S11). Therefore, we attribute the dispersion in the TIP4P-FB molar fraction profiles in Fig. 4(a) to random variation among replicates and rationalize the continued use of Eq. (6) to isolate the inversion temperature of TIP4P-FB.

The predicted inversion temperatures of each water model are summarized in Fig. 4(b). TIP3P-FB reproduced an inversion temperature of $11 \pm 1\,^{\circ}\mathrm{C}$, closest to the experimental value. TIP4P-FB and OPC3 predicted the next closest inversion temperatures of $6 \pm 3\,^{\circ}\mathrm{C}$ and $6 \pm 2\,^{\circ}\mathrm{C}$, respectively; SPC/E followed, predicting $-2 \pm 2\,^{\circ}\mathrm{C}$; and OPC predicted $-6 \pm 8\,^{\circ}\mathrm{C}$, furthest from the experimental value. The large uncertainty in the inversion temperature of OPC was likely due to the temperature range of the simulation not having centrally encompassed a clear maximum in the molar fraction curve.

C. Soret coefficients

The Soret coefficient is essentially a cross-coupling coefficient that describes the interplay between a thermal gradient and a mass flux. The magnitude of the Soret coefficient of aqueous ionic solutions is typically quite small (on the order of 1×10^{-3} K^{-1}), and it is therefore much more difficult to measure than direct coefficients, such as self-diffusion or thermal expansion.[51] To determine how well each water model predicts the Soret coefficient of $[\mathrm{NaCl}]_{aq}$ solutions, we constructed a suite of simulations that span a temperature range of $5\,^{\circ}\mathrm{C} < T < 95\,^{\circ}\mathrm{C}$ at average concentrations of 0.5, 2, and 4 M (equivalently 0.53, 2.24, and 4.88 mol kg^{-1} respectively). The Soret coefficients obtained from these simulations were compared directly to experimental values in comparable conditions sourced from Ref. 12 at 0.5, 2, and 4 mol kg^{-1}. The Soret coefficient changes minimally between these corresponding concentrations of molality and molarity, particularly for 0.5 mol kg^{-1} solutions and the 2 and 4 mol kg^{-1} solutions with an average temperature of $45\,^{\circ}\mathrm{C}$ (see Fig. S6). While this difference in concentration between laboratory measures and simulation measures is not ideal, it is does not affect the assessment of a water model's performance in reproducing thermodiffusion made in this work.

The average fitted molar fraction profile of each water model from 0.5 M NaCl simulations with a temperature range of $[5, 55]\,^{\circ}\mathrm{C}$ is shown in Fig. 5 as an example of the typical results obtained. The fitted molar fraction profile of each of the three replicates of this simulation is included in Fig. S7. Simulations from all concentration and temperature ranges listed in Table I were analyzed in the same way and are included in Figs. S8–S11. Figure 5 shows that all water models, except TIP3P, had distinct curvature in their molar fraction profiles and, therefore, predicted temperature dependent thermodiffusion. As with the inversion temperature simulations, TIP3P predicted a linear molar fraction profile.

The temperature range $[5, 55]\,^{\circ}\mathrm{C}$ encompasses the expected inversion temperature of $T_0 \approx 10\,^{\circ}\mathrm{C}$, so the molar fraction profiles might be expected to show a maximum near $10\,^{\circ}\mathrm{C}$. Indeed, all water models, except TIP3P, showed a distinct curvature at the lower temperature end of the molar fraction profile that is captured by the curve fit. However, the temperature range did not extend low enough to have confidently placed the temperature at which the curve achieves its maximum.

The Soret coefficients of each water model across the full temperature and concentration ranges tested are shown in Fig. 6. Water models predicted different Soret coefficients and, hence, different thermodiffusive behavior of the ions in the solution. In general, the TIP3P-FB water model appears to have predicted the Soret coefficient closest to the experimental values, while the TIP3P water model had the largest disagreement with the experimental values. Across the different NaCl concentrations, it appears that the TIPnP-FB and OPCn water model families predicted Soret coefficients in 0.5 and 2 M solutions more accurately than in 4 M solutions.

Insight into the performance of the water models for 0.5 M NaCl across the full temperature range was gained by observing the Soret coefficients measured at each simulation average temperature in Fig. 7, including the results from the inversion simulations. All water models, except TIP3P, showed temperature dependent Soret coefficients that reasonably followed the empirical functional form for $S_T(T)$, i.e., Eq. (7). TIPnP-FB, SPC/E and OPCn water models confidently recreate the qualitative change in Soret coefficient with temperature. Therefore, these water models are recreating the

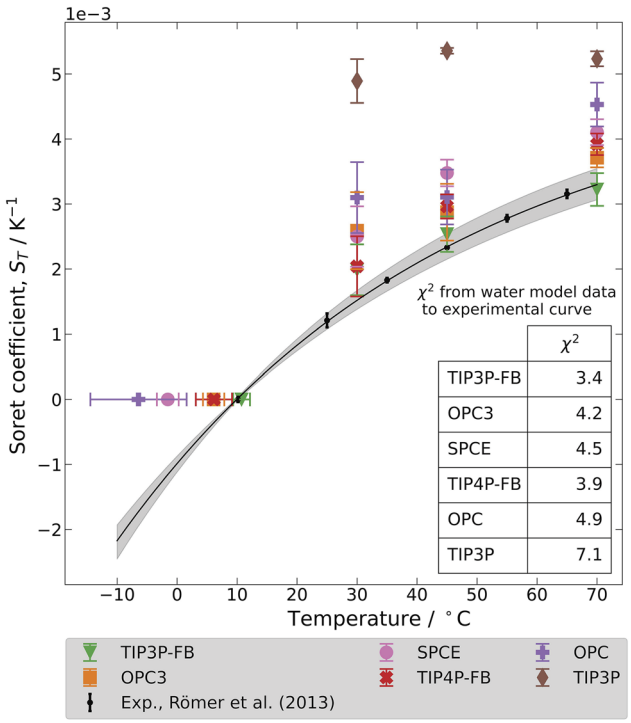

FIG. 7. Soret coefficient and inversion temperature in 0.5 M NaCl (0.53 mol kg^{-1}) solutions as a function of temperature for each water model. Experimental data from Ref. 12 is shown in black for the comparable concentration of 0.5 mol kg^{-1} NaCl and fit to the $S_T(T)$ functional form from Eq. (7), with maximum error in the fit shaded in gray. A measure of distance between the predictions of each water model and the experimental curve is quantified by a χ^2 value in the right-hand side table, where smaller χ^2 values imply the water models predictions are closer to the experimental curve.

25 March 2024 00:54:31

Published under an exclusive license by AIP Publishing

dynamics and behavior of water and ion molecules that result in a complex thermodiffusive transport of electrolytic species, displaying both thermophobic and thermophilic diffusion with an inversion value.

IV. DISCUSSION

A. How well did each water model perform?

As hypothesized, the water model impacted the thermodiffusive behavior of the modeled NaCl solutions. Simulations with all rigid non-polarizable water models were able to qualitatively reproduce thermodiffusion. All water models, except TIP3P, predicted an inversion temperature in a 0.5 M NaCl solution [Fig. 4(b)], with the ions showing thermophilic and thermophobic behavior within the non-isothermal calculation domain [Fig. 4(a)]. Furthermore, water models of the TIPnP-FB, SPC/E, and OPCn families were able to recreate the increase in the Soret coefficient with temperature with reasonably accurate quantitative predictions when compared to the laboratory-based measurements of Römer *et al.*[12] at comparable concentrations (Fig. 6). The most accurate quantitative predictions of thermodiffusion in the temperature range of $[-10, 70]\,^{\circ}\mathrm{C}$ were obtained with TIP3P-FB, followed by TIP4P-FB and OPC3 for a 0.5 M NaCl solution (Fig. 7).

The tested water models differed by the number of atoms in their molecular structure and the reference data that they were parameterized against. The success of the models being able to recreate complex thermodiffusive behavior is notable, given that thermodiffusion was not part of the reference data for any of the water models. Therefore, parameterization of a new water model that includes thermodiffusion reference data, e.g., via the ForceBalance methodology,[35] can improve the accuracy in the quantitative prediction of thermodiffusion. However, with the time consuming nature of predicting thermodiffusion coefficients using MD, tuning new models could be a very computationally expensive venture, while the reasonable accuracy of the TIP3P-FB water model (and indeed the TIPnP-FB and OPCn families) to predict Soret coefficients encourages further assessment with more salts and other types of binary mixtures.

1. TIP3P

TIP3P was undoubtedly the worst performing water model in our study, consistently predicting linear molar fraction profiles of the ions with temperature [Fig. 4(a)]. This result demonstrates that either TIP3P is incapable of modeling temperature-dependent behavior or it predicts an inversion temperature for NaCl far outside the range explored in this study. TIP3P is a relatively old water model with a limited set of reference data, e.g. the density of water at $25\,^{\circ}\mathrm{C}$.[38] It may not be surprising that TIP3P cannot predict the temperature-dependent thermodiffusive behavior, given that no temperature dependence is included in its reference data. The poor performance of TIP3P, however, has broader implications to future simulations of thermodiffusion and thermophoresis. TIP3P is the default water model for the Chemistry at Harvard Molecular Mechanics (CHARMM) force field,[38] so many biologically relevant molecules and atoms have been parameterized against it. Poor results are likely to be obtained in simulations of thermophoresis for biomolecules when implementing CHARMM force fields with the TIP3P water model. Better results may be obtained with biomolecular force fields that use other water models (e.g. AMBER ff19 with OPC), so further testing on the compatibility of the CHARMM force field with different water models, such as TIP3P-FB (as in Ref. 52) is required.

2. SPC/E

SPC/E has been the most commonly used water model for MD simulations of thermodiffusion, e.g., see Refs. 12, 31, and 32. Although this model reproduced the expected qualitative behavior, neither our nor other simulations, gave precise quantitative results. We found that SPC/E predicted an inversion temperature for $0.53\ \mathrm{mol\ kg^{-1}}$ NaCl of $-2 \pm 2\,^{\circ}\mathrm{C}$ at 1.013 bar. Direct comparison with previous simulations is difficult due to the use of different conditions. Römer *et al.*[12] predicted an inversion temperature of around $26\,^{\circ}\mathrm{C}$ for a $2.5\ \mathrm{mol\ kg^{-1}}$ at 100 bar with identical ion parameters, while Di Lecce and Bresme[31] with almost identical ion parameters (only a small difference in the ϵ value of the Cl^- parameters) found an inversion temperature of $-8\,^{\circ}\mathrm{C}$ for a $2.0\ \mathrm{mol\ kg^{-1}}$ at 600 bar. Extrapolated laboratory-based measurements for the inversion temperatures are $10.0 \pm 0.2\,^{\circ}\mathrm{C}$ for $0.5\ \mathrm{mol\ kg^{-1}}$ and $-5 \pm 6\,^{\circ}\mathrm{C}$ for $2.0\ \mathrm{mol\ kg^{-1}}$. Although it has been stated that pressure has only a small influence on the predicted Soret coefficients[12,31,32] in the range of 100–600 bar, the dependence of inversion temperature on pressure has not been fully characterized. We found that SPC/E performed better at higher NaCl concentrations (Fig. 6).

3. TIPnP-FB and OPCn

The TIPnP-FB and OPCn water models could all qualitatively predict the temperature-dependent Soret coefficient, with TIP3P-FB overall yielding values closest to those measured in the laboratory. Therefore, these water models can recreate the dynamics and behavior of water and ion molecules that display complex thermodiffusion. Surprisingly, there was no advantage of the four-point model over its three-point counterpart, despite TIP4P-FB and OPC models generally being found to perform better at predicting standard properties of water than TIP3P-FB and OPC3.[36,37] Our result is similar to the observation that four-point water models do not have an advantage over three-point water models in their ability to model heat conduction.[53,54] Our data showed that the TIPnP-FB water model family performed better than the OPCn family. The TIPnP-FB family is parameterized against a large dataset of water properties measured over a large range of temperatures and pressures, as well as small amount of molecule data generated by quantum mechanics calculations. It is therefore expected that the TIPnP-FB water models can recreate temperature-dependent behavior. The OPCn family has a stronger focus on the electrostatic potential of a water molecule obtained from quantum mechanical calculations, so it is a more fundamental theoretical approximation that can recreate temperature-dependent properties in aqueous solutions.

B. Why do water models perform differently?

It is not entirely clear why any of the TIPnP-FB, OPCn, or SPC/E water models performed better than any other. By comparing with the works of Wang *et al.*[35] and Izadi *et al.*,[36,37] we see that these water models reproduce standard properties of water well (self-diffusion, density, heat of vaporization, isothermal compressibility,

25 March 2024 00:54:31

Published under an exclusive license by AIP Publishing

isobaric heat capacity, dielectric constant, sheer viscosity, radial distribution functions for O–O and O–H, and thermal expansion) and with comparable accuracy. There does not appear to be any obvious correlation between their performance in reproducing standard water properties and with their performance in reproducing thermodiffusion. In particular, while TIP3P-FB predicts these standard properties of water well, it does not generally perform better than the four-point models OPC and TIP4P-FB, or the three-point model OPC3.

In this work, the thermodiffusive performance based on the combined water and ion model pair was assessed, not only the independent water model. A standard property that is reproduced by the combined water and ion models is the solution density. We have found that the water and ion model pairs used in this study reproduce the changes in density of the NaCl solutions across temperature and concentration well (see Fig. S13). However, TIP3P-FB was not the most accurate for this task. TIP4P-FB most accurately and consistently reproduced solution density of the TIPnP-FB, OPCn, and SPC/E water models, and OPC3 the least accurately. This result demonstrates that the ion parameters influence the predicted solution density, since OPC is the most accurate at predicting the density of pure water (see Fig. S14), but TIP4P-FB is the most accurate at predicting the NaCl solution densities. However, it appears that water and ion models' ability to reproduce the density of a solution is not indicative of their ability to reproduce the Soret coefficient.

It is possible that another set of ion parameters could change the thermodiffusive behavior and performance reported here for the water models (even TIP3P). Previous studies have shown a small dependence of inversion temperature and Soret coefficient on the ion parameter choice.[12,31] In our case, we focused on a single set of ion parameters for each water model, each optimized in the same way to recreate the hydration free energy in 0.3 M cation–anion pair solutions.[40] Despite the ion parameters being optimized in the same way, there were reported differences in the overall performance of the ions for each water model in their ability to recreate the hydration free energy and ion–oxygen distance of Na^+ and Cl^-.[40,41] The ion hydration free energy predicted by each combined water and ion model used in this study is reported in Table II. In general, the ions of three-point water models were more accurate in reproducing ion hydration free energies than their four-point counterparts (i.e. TIP3P-FB was more accurate than TIP4P-FB), TIPnP-FB models were more accurate than OPCn models (for the same n-point model), SPC/E had reasonably accurate ions, and TIP3P had the least accurate ions. These trends roughly reproduce the accuracy of the water models in predicting thermodiffusive behavior, suggesting that the overall accuracy of the ion model is an important factor in determining how well thermodiffusion is modeled. Nonetheless, we find it encouraging that we obtained good results without the need to consider thermodiffusion in the ion or water parameterization. We note that the choice of ion parameters can also explain why our Soret coefficient predictions of the 0.5 and 2.0 M NaCl solutions are much closer to the experimental values than those predicted for the 4.0 M solutions (Fig. 6). This is likely due to the ion concentration of 4.0 M being far outside of the parameterized range.

TABLE II. Hydration free energies (HFEs) of Na^+ and Cl^- ions predicted by each combined water and ion model used in this study, compared to experimental values. Experimental HFE sourced for Na^+ from Ref. 55 and for Cl^- from Ref. 56. Predicted hydration free energies sourced for TIP3P-FB, OPC3, TIP4P-FB, and OPC from SI of Ref. 40 and for TIP3P and SPC/E from Ref. 41.

	Na^+ HFE (kcal mol^{-1})	Cl^- HFE (kcal mol^{-1})
Experimental	−87.2	−89.1
TIP3P-FB	−87.2	−89.1
OPC3	−87.1	−89.0
TIP4P-FB	−87.5	−89.4
OPC	−86.6	−89.2
SPC/E	−87.2	−87.8
TIP3P	−88.7	−89.6

C. Implications of water model performance

We note that a water model's ability to recreate thermodiffusion is not reflective of its overall performance in recreating other phenomena. It is expected that an MD water model will be able to produce certain properties better than others, with greater accuracy in reproducing the properties in their reference data. The choice of which water model to use in a simulation is guided by the properties that the researcher decides are important for their phenomena of interest. Because of this, multiple works assess the abilities of different water models to recreate a wide variety of important water properties.[36,37,57] Notably, the recent 2021 publication of Pathirannahalage *et al.*[57] comprehensively compares performance of 30 commonly used water models to assist researchers with this decision. In fact, OPC is the best general performing water model of the TIPnP-FB and OPCn families.[36,37] That TIP3P-FB performed best for modeling thermodiffusion in aqueous NaCl solutions does not imply it will be better than the other tested water models for all solutes in all conditions of temperature, pressure, and concentration. Indeed, the temperature and concentration dependence of thermodiffusion in more aqueous electrolyte mixtures would need to be studied for a more general water model recommendation to be made. In particular, aqueous KCl and KBr solutions would make good candidates for further simulation as laboratory measures of their Soret coefficients and inversion temperatures are already available.[3,12] Another direction for future work would be to examine how well other force fields could replicate thermophoresis, including polarizable potentials and fixed charge models with scaled ionic charges that have proven able to reproduce many properties of aqueous electrolyte solutions.[58,59]

V. CONCLUSIONS

All tested rigid non-polarizable water models qualitatively reproduced thermodiffusive behavior. Simulations using TIP3P-FB, followed by TIP4P-FB and OPC3, resulted in the most accurate quantitative predictions of thermodiffusion in the temperature range $[-10, 70]\,^{\circ}\mathrm{C}$ for a 0.5 M NaCl solution. However, all of the TIPnP-FB, OPCn and SPC/E water models predicted a temperature at which the thermal preference of ions switch in 0.5 M NaCl solution and could predict the increase in the Soret coefficient with temperature with reasonable accuracy when compared

25 March 2024 00:54:31

Published under an exclusive license by AIP Publishing

to the laboratory-based measurements of Römer *et al.*[12] More accurate thermodiffusion predictions were obtained by using combined water and ion models that accurately recreate standard properties of the ion–water interactions, such as hydration free energy and ion–oxygen distance, rather than standard properties of water.

Our results provide guidance for the choice of water and ion models to use in future simulations of thermodiffusion in aqueous NaCl solutions. Importantly, the results provide further confidence that such simulations can capture molecular scale details of the interaction between ions and water molecules to achieve a better understanding and predictions of thermodiffusive behavior. A limitation in our study is that we could only compare to experimental data from one source due to the lack of such laboratory-based measurements. Future experiments that characterized thermodiffusion for a number of binary electrolyte mixtures across a range of temperatures and concentrations would allow for more complete validation of the simulation predictions. Interestingly, the different performances of the water models could help explain the mechanisms of temperature sensitive thermodiffusion. Future directions of this work could focus on exploring the fundamental reasons why different water models yield varying thermodiffusive predictions.

SUPPLEMENTARY MATERIAL

The supplementary material contains tables of the parameters of the water and ion models used in this study and the boundary conditions of parameters for fitting the molar fraction against temperature data. Graphs of the calibrated temperature profiles of each simulation environment, the effect of thermostat width on the temperature profile, the effect of the equilibration time on the inversion temperature, convergence of the temperature and ion concentration profiles, and the influence of solution concentration on the Soret coefficient are included. The supplementary information also contains the molar fraction profiles obtained from each simulation environment, a more in-depth fitting of the predicted Soret coefficients of 0.5 M NaCl solutions over temperature, the density of the NaCl solutions across temperature and concentration, and the density of water predicted by each water model used in this study.

ACKNOWLEDGMENTS

The authors acknowledge funding from the Foundation for Australia-Japan Studies. This research/project was undertaken with the assistance of resources and services from the National Computational Infrastructure (NCI), which is supported by the Australian Government. The authors declare no competing interests.

AUTHOR DECLARATIONS

Conflict of Interest

The authors have no conflicts to disclose.

DATA AVAILABILITY

The data that support the findings of this study are available from the corresponding author upon reasonable request.

REFERENCES

[1] S. R. De Groot and P. Mazur, *Non-Equilibrium Thermodynamics* (Dover, New York, 1984).
[2] M. A. Rahman and M. Z. Saghir, "Thermodiffusion or Soret effect: Historical review," Int. J. Heat Mass Transfer **73**, 693–705 (2014).
[3] S. Mohanakumar, J. Luettmer-Strathmann, and S. Wiegand, "Thermodiffusion of aqueous solutions of various potassium salts," J. Chem. Phys. **154**, 084506 (2021).
[4] D. R. Caldwell and S. A. Eide, "Separation of seawater by Soret diffusion," Deep-Sea Res., Part A **32**, 965–982 (1985).
[5] S. A. Putnam, D. G. Cahill, and G. C. L. Wong, "Temperature dependence of thermodiffusion in aqueous suspensions of charged nanoparticles," Langmuir **23**, 9221–9228 (2007).
[6] M. F. Riley and A. Firoozabadi, "Compositional variation in hydrocarbon reservoirs with natural convection and diffusion," AIChE J. **44**, 452–464 (1998).
[7] M. A. Gallis, D. J. Rader, and J. R. Torczynski, "Thermophoresis in rarefied gas flows," Aerosol Sci. Technol. **36**, 1099–1117 (2002).
[8] V. V. Shumova, D. N. Polyakov, and L. M. Vasilyak, "Thermophoresis in plasma with structures of charged dust particles," Russ. J. Phys. Chem. B **14**, 666–669 (2020).
[9] C. Liu, J. Zhao, F. Tian, L. Cai, W. Zhang, Q. Feng, J. Chang, F. Wan, Y. Yang, B. Dai *et al.*, "Low-cost thermophoretic profiling of extracellular-vesicle surface proteins for the early detection and classification of cancers," Nat. Biomed. Eng. **3**, 183–193 (2019).
[10] B. Cameron Reed, "Liquid thermal diffusion during the manhattan project," Phys. Perspect. **13**, 161–188 (2011).
[11] D. R. Caldwell, "Thermal and Fickian diffusion of sodium chloride in a solution of oceanic concentration," Deep-Sea Res. Oceanogr. Abstr. **20**, 1029–1039 (1973).
[12] F. Römer, Z. Wang, S. Wiegand, and F. Bresme, "Alkali halide solutions under thermal gradients: Soret coefficients and heat transfer mechanisms," J. Phys. Chem. B **117**, 8209–8222 (2013).
[13] B.-J. De Gans, R. Kita, B. Müller, and S. Wiegand, "Negative thermodiffusion of polymers and colloids in solvent mixtures," J. Chem. Phys. **118**, 8073–8081 (2003).
[14] S. Iacopini, R. Rusconi, and R. Piazza, "The "macromolecular tourist": Universal temperature dependence of thermal diffusion in aqueous colloidal suspensions," Eur. Phys. J. E **19**, 59–67 (2006).
[15] D. Vigolo, R. Rusconi, H. A. Stone, and R. Piazza, "Thermophoresis: microfluidics characterization and separation," Soft Matter **6**, 3489–3493 (2010).
[16] A. Würger, "Thermal non-equilibrium transport in colloids," Rep. Prog. Phys. **73**, 126601 (2010).
[17] R. Cabreira Gomes, A. Ferreira Da Silva, M. Kouyaté, G. Demouchy, G. Mériguet, R. Aquino, E. Dubois, S. Nakamae, M. Roger, J. Depeyrot, and R. Perzynski, "Thermodiffusion of repulsive charged nanoparticles-the interplay between single-particle and thermoelectric contributions," Phys. Chem. Chem. Phys. **20**, 16402–16413 (2018).
[18] J. F. Torres, A. Komiya, D. Henry, and S. Maruyama, "Measurement of Soret and Fickian diffusion coefficients by orthogonal phase-shifting interferometry and its application to protein aqueous solutions," J. Chem. Phys. **139**, 074203 (2013).
[19] S. Iacopini and R. Piazza, "Thermophoresis in protein solutions," Europhys. Lett. **63**, 247–253 (2003).
[20] S. Duhr and D. Braun, "Why molecules move along a temperature gradient," Proc. Natl. Acad. Sci. U. S. A. **103**, 19678–19682 (2006).
[21] E. L. Talbot, J. Kotar, L. Parolini, L. Di Michele, and P. Cicuta, "Thermophoretic migration of vesicles depends on mean temperature and head group chemistry," Nat. Commun. **8**, 15351–15358 (2017).
[22] R. De Miguel and J. M. Rubí, "Negative thermophoretic force in the strong coupling regime," Phys. Rev. Lett. **123**, 200602 (2019).
[23] S. Hoda, S. Srinivasan, and M. Z. Saghir, "Thermodiffusion in binary and ternary hydrocarbon mixtures studied using a modified heat exchange algorithm," Therm. Sci. Eng. Prog. **4**, 168–174 (2017).
[24] J.-M. Simon, D. K. Dysthe, A. H. Fuchs, and B. Rousseau, "Thermal diffusion in alkane binary mixtures: A molecular dynamics approach," Fluid Phase Equilib. **150–151**, 151–159 (1998).

25 March 2024 00:54:31

Published under an exclusive license by AIP Publishing

[25]A. Perronace, C. Leppla, F. Leroy, B. Rousseau, and S. Wiegand, "Soret and mass diffusion measurements and molecular dynamics simulations of *n*-pentane-*n*-decane mixtures," J. Chem. Phys. **116**, 3718–3729 (2002).
[26]M. Zhang and F. Müller-Plathe, "Reverse nonequilibrium molecular-dynamics calculation of the Soret coefficient in liquid benzene/cyclohexane mixtures," J. Chem. Phys. **123**, 124502 (2005).
[27]A. Perronace, G. Ciccotti, F. Leroy, A. H. Fuchs, and B. Rousseau, "Soret coefficient for liquid argon-krypton mixtures via equilibrium and nonequilibrium molecular dynamics: A comparison with experiments," Phys. Rev. E **66**, 031201 (2002).
[28]C. Nieto-Draghi, J. B. Avalos, and B. Rousseau, "Computing the Soret coefficient in aqueous mixtures using boundary driven nonequilibrium molecular dynamics," J. Chem. Phys. **122**, 114503 (2005).
[29]A. Diaz-Marquez and G. Stirnemann, "Silico all-atom approach to thermodiffusion in dilute aqueous solutions," J. Chem. Phys. **155**, 174503 (2021).
[30]M. Belkin, S.-H. Chao, G. Giannetti, and A. Aksimentiev, "Modelling thermophoretic effects in solid-state nanopores," Comput. Electron. **13**, 826–838 (2014).
[31]S. Di Lecce and F. Bresme, "Soret coefficients and thermal conductivities of alkali halide aqueous solutions via non-equilibrium molecular dynamics simulations," Mol. Simul. **45**, 351–357 (2019).
[32]S. Di Lecce, T. Albrecht, and F. Bresme, "The role of ion-water interactions in determining the Soret coefficient of LiCl aqueous solutions," Phys. Chem. Chem. Phys. **19**, 9575–9583 (2017).
[33]D. Niether, S. Di Lecce, F. Bresme, and S. Wiegand, "Unravelling the hydrophobicity of urea in water using thermodiffusion: Implications for protein denaturation," Phys. Chem. Chem. Phys. **20**, 1012–1020 (2018).
[34]D. Niether and S. Wiegand, "Thermophoresis of biological and biocompatible compounds in aqueous solution," J. Phys.: Condens. Matter **31**, 503003 (2019).
[35]L.-P. Wang, T. J. Martinez, and V. S. Pande, "Building force fields: An automatic, systematic, and reproducible approach," J. Phys. Chem. Lett. **5**, 1885–1891 (2014).
[36]S. Izadi, R. Anandakrishnan, and A. V. Onufriev, "Building water models: A different approach," Am. Chem. Soc. **5**, 3863–3871 (2014).
[37]S. Izadi and A. V. Onufriev, "Accuracy limit of rigid 3-point water models," J. Chem. Phys. **145**, 074501 (2016).
[38]J. Huang and A. D. MacKerell, Jr., "CHARMM36 all-atom additive protein force field: Validation based on comparison to NMR data," J. Comput. Chem. **34**, 2135–2145 (2013).
[39]H. J. C. Berendsen, J. R. Grigera, and T. P. Straatsma, "The missing term in effective pair potentials," J. Phys. Chem. **91**, 6269–6271 (1987).
[40]A. Sengupta, Z. Li, L. F. Song, P. Li, and K. M. Merz, "Parameterization of monovalent ions for the OPC3, OPC, TIP3P-FB, and TIP4P-FB water models," J. Chem. Inf. Model. **61**, 869–880 (2021).
[41]I. S. Joung and T. E. Cheatham, "Determination of alkali and halide monovalent ion parameters for use in explicitly solvated biomolecular simulations," J. Phys. Chem. B **112**, 9020–9041 (2008).
[42]L. X. Dang, "Development of nonadditive intermolecular potentials using molecular dynamics: Solvation of Li^+ and F^- ions in polarizable water," J. Chem. Phys. **96**, 6970–6977 (1992).
[43]L. X. Dang and B. C. Garrett, "Photoelectron spectra of the hydrated iodine anion from molecular dynamics simulations," J. Chem. Phys. **99**, 2972–2977 (1993).
[44]D. E. Smith and L. X. Dang, "Computer simulations of NaCl association in polarizable water," J. Chem. Phys. **100**, 3757–3766 (1994).
[45]L. X. Dang, "Mechanism and thermodynamics of ion selectivity in aqueous solutions of 18-crown-6 ether: A molecular dynamics study," J. Am. Chem. Soc. **117**, 6954–6960 (1995).
[46]F. Bresme and J. Armstrong, "Note: Local thermal conductivities from boundary driven non-equilibrium molecular dynamics simulations," J. Chem. Phys. **140**, 016102 (2014).
[47]J. C. Phillips, D. J. Hardy, J. D. Maia, J. E. Stone, J. V. Ribeiro, R. C. Bernardi, R. Buch, G. Fiorin, J. Hénin, W. Jiang, R. McGreevy, M. C. Melo, B. K. Radak, R. D. Skeel, A. Singharoy, Y. Wang, B. Roux, A. Aksimentiev, Z. Luthey-Schulten, L. V. Kalé, K. Schulten, C. Chipot, and E. Tajkhorshid, "Scalable molecular dynamics on CPU and GPU architectures with NAMD," J. Chem. Phys. **153**, 044130 (2020).
[48]M. R. Shirts and J. D. Chodera, "Statistically optimal analysis of samples from multiple equilibrium states," J. Chem. Phys. **129**, 124105 (2008).
[49]J. D. Chodera, W. C. Swope, J. W. Pitera, C. Seok, and K. A. Dill, "Use of the weighted histogram analysis method for the analysis of simulated and parallel tempering simulations," J. Chem. Theory Comput. **3**, 26–41 (2007).
[50]T. Kluyver, B. Ragan-Kelley, F. Pérez, B. Granger, M. Bussonnier, J. Frederic, K. Kelley, J. Hamrick, J. Grout, S. Corlay, P. Ivanov, D. Avila, S. Abdalla, and C. Willing, "Jupyter notebooks—A publishing format for reproducible computational workflows," in *Positioning and Power in Academic Publishing: Players, Agents and Agendas - Proceedings of the 20th International Conference on Electronic Publishing* (ELPUB, 2016), pp. 87–90.
[51]P.-A. Artola and B. Rousseau, "Thermal diffusion in simple liquid mixtures: What have we learnt from molecular dynamics simulations?," Mol. Phys. **111**, 3394–3403 (2013).
[52]F. Sajadi and C. N. Rowley, "Simulations of lipid bilayers using the CHARMM36 force field with the TIP3P-FB and TIP4P-FB water models," PeerJ **6**, e5472 (2018).
[53]F. Römer, A. Lervik, and F. Bresme, "Nonequilibrium molecular dynamics simulations of the thermal conductivity of water: A systematic investigation of the SPC/E and TIP4P/2005 models," J. Chem. Phys. **137**, 074503 (2012).
[54]T. W. Sirk, S. Moore, and E. F. Brown, "Characteristics of thermal conductivity in classical water models," J. Chem. Phys. **138**, 064505 (2013).
[55]Y. Marcus, "Thermodynamics of solvation of ions. Part 5.—Gibbs free energy of hydration at 298.15 K," J. Chem. Soc., Faraday Trans. **87**, 2995–2999 (1991).
[56]R. Schmid, A. M. Miah, and V. N. Sapunov, "A new table of the thermodynamic quantities of ionic hydration: Values and some applications (enthalpy–entropy compensation and Born radii)," Phys. Chem. Chem. Phys. **2**, 97–102 (2000).
[57]S. P. K. Pathirannahalage, N. Meftahi, A. Elbourne, A. C. G. Weiss, C. F. McConville, A. Padua, D. A. Winkler, M. C. Gomes, T. L. Greaves, T. C. Le, Q. A. Besford, and A. J. Christofferson, "Systematic comparison of the structural and dynamic properties of commonly used water models for molecular dynamics simulations," J. Chem. Inf. Modell. **61**, 4521 (2021).
[58]J. L. F. Abascal and C. Vega, "A general purpose model for the condensed phases of water: TIP4P/2005," J. Chem. Phys. **123**, 234505 (2005).
[59]I. M. Zeron, J. L. F. Abascal, and C. Vega, "A force field of Li^+, Na^+, K^+, Mg^{2+}, Ca^{2+}, Cl^-, and SO_4^{2-} in aqueous solution based on the TIP4P/2005 water model and scaled charges for the ions," J. Chem. Phys. **151**, 134504 (2019).

25 March 2024 00:54:31

Published under an exclusive license by AIP Publishing